Monthly Notices
of the
ROYAL ASTRONOMICAL SOCIETY

MNRAS **465,** 3817–3822 (2017)
Advance Access publication 2016 November 5

doi:10.1093/mnras/stw2864

The VIMOS Public Extragalactic Redshift Survey (VIPERS): galaxy segregation inside filaments at $z \simeq 0.7$

N. Malavasi,[1,2⋆] S. Arnouts,[2] D. Vibert,[2] S. de la Torre,[2] T. Moutard,[2] C. Pichon,[3,4] I. Davidzon,[2] K. Kraljic,[2] M. Bolzonella,[5] L. Guzzo,[6,7] B. Garilli,[8] M. Scodeggio,[8] B. R. Granett,[6,7] U. Abbas,[9] C. Adami,[2] D. Bottini,[8] A. Cappi,[5,10] O. Cucciati,[1,5] P. Franzetti,[8] A. Fritz,[8] A. Iovino,[6] J. Krywult,[11] V. Le Brun,[2] O. Le Fèvre,[2] D. Maccagni,[8] K. Małek,[12] F. Marulli,[1,5,13] M. Polletta,[8,14,15] A. Pollo,[12,16] L. Tasca,[2] R. Tojeiro,[17] D. Vergani,[18] A. Zanichelli,[19] J. Bel,[20] E. Branchini,[21,22,23] J. Coupon,[24] G. De Lucia,[25] Y. Dubois,[3] A. Hawken,[6] O. Ilbert,[2] C. Laigle,[3] L. Moscardini,[1,5,13] T. Sousbie,[3] M. Treyer[2] and G. Zamorani[5]

Affiliations are listed at the end of the paper

Accepted 2016 November 2. Received 2016 November 2; in original form 2016 September 14

ABSTRACT

We present the first quantitative detection of large-scale filamentary structure at $z \simeq 0.7$ in the large cosmological volume probed by the VIMOS Public Extragalactic Redshift Survey (VIPERS). We use simulations to show the capability of VIPERS to recover robust topological features in the galaxy distribution, in particular the filamentary network. We then investigate how galaxies with different stellar masses and stellar activities are distributed around the filaments, and find a significant segregation, with the most massive or quiescent galaxies being closer to the filament axis than less massive or active galaxies. The signal persists even after downweighting the contribution of peak regions. Our results suggest that massive and quiescent galaxies assemble their stellar mass through successive mergers during their migration along filaments towards the nodes of the cosmic web. On the other hand, low-mass star-forming galaxies prefer the outer edge of filaments, a vorticity-rich region dominated by smooth accretion, as predicted by the recent spin alignment theory. This emphasizes the role of large-scale cosmic flows in shaping galaxy properties.

Key words: galaxies: evolution – galaxies: high-redshift – galaxies: statistics – cosmology: observations – large-scale structure of Universe.

1 INTRODUCTION

A major success of the Λ cold dark matter (ΛCDM) model is its ability to reproduce the wealth of large-scale structures (LSSs) observed in the galaxy distribution (e.g. Springel, Frenk & White 2006). These structures arise from the growth of primordial, nearly Gaussian, matter density fluctuations under the effect of gravity. In this process, matter departs from underdense regions and flows through dense sheets that wind up, forming filaments along which matter drifts, and progressively gets accreted on to high-density peaks. This leads to a cosmic web (CW) where dense nodes are connected by filaments, framing walls separated by large voids (Bond, Kofman & Pogosyan 1996). The baryonic gas follows the gravitational potential gradients imposed by the dark matter distribution, and is then shocked, forming (among other structures) tenuous ionized hydrogen filaments, the intergalactic medium (IGM), in which galaxies can form. These filaments are regions where gas, momentum, and energy are exchanged through the complex processes of infall and outflow. While it has long been established that the local density environment on typical scales below a few Mpc plays a role in shaping galaxy properties (see e.g. Dressler 1980; Zehavi et al. 2005), the extent to which large-scale anisotropic structures and the tidal field of the CW influence the evolution of galaxies (and subsequently properties such as morphology, accretion mode, and merging rate) still remains an open issue.

There is significant numerical evidence that a large-scale environment has an impact on the formation and evolution of galaxies.

⋆ E-mail: nicola.malavasi@lam.fr

© 2016 The Authors
Published by Oxford University Press on behalf of the Royal Astronomical Society

Downloaded from https://academic.oup.com/mnras/article-abstract/465/4/3817/2420717 by guest on 10 July 2020

In particular, *N*-body dark matter simulations have shown that the spin and the shape of dark matter haloes depend on the large-scale environment in which they reside (Aragón-Calvo et al. 2007; Hahn et al. 2007; Sousbie, Colombi & Pichon 2009). Moreover, using hydrodynamical simulations, Kereš et al. (2005) found that at high redshifts cold streams can penetrate deep inside haloes and feed galaxies with fresh gas to sustain intense star formation (SF) activity (see also Dekel & Birnboim 2006; Dekel et al. 2009). Pichon et al. (2011) proposed that the filamentary flows advect angular momentum on to the discs of galaxies and that the spin of newly formed galaxies tends preferentially to be parallel to the axis of their closest filament. Codis et al. (2012) quantified a mass transition, with the most massive haloes ending up with a spin perpendicular to the filaments as a result of successive mergers along the filaments. These results have been extended to galaxies by Dubois et al. (2014) with the state-of-the-art hydrodynamical simulation Horizon-AGN (see also Codis, Pichon & Pogosyan 2015, for a theoretical motivation for this transition based on constrained tidal torque theory). On the side of observations, the correlation between the spin of galaxies and their filaments or sheets has been recently detected in the Sloan Digital Sky Survey (SDSS; Trujillo, Carretero & Patiri 2006; Tempel, Stoica & Saar 2013; Zhang et al. 2013). This remarkable result confirms the role played by the large-scale dynamical environment in the evolution of galaxies,[1] which is usually neglected in galaxy formation models (e.g. Zehavi et al. 2005; Guo et al. 2011).

In the local Universe ($z \leq 0.3$), the large galaxy redshift surveys 2dF (Colless et al. 2001), SDSS (York et al. 2000), and GAMA (Driver et al. 2011) have captured the CW in great detail and led to several analyses showing variations of individual (Beygu et al. 2013; Alpaslan et al. 2015, 2016) and statistical (Eardley et al. 2015; Martínez, Muriel & Coenda 2016) galaxy properties as a function of their CW environment. At higher redshifts, because of the small volumes probed and the low sampling rates achieved by redshift surveys, this kind of analysis has not been possible until recently. The state-of-the-art redshift survey VIMOS Public Extragalactic Redshift Survey (VIPERS; Guzzo et al. 2014) overcomes these limitations by probing a volume equivalent to the local 2dF survey with a dense spectroscopic sampling of galaxies. It allowed the first measurement of the growth rate of the LSS at $0.5 \leq z \leq 1.2$ (de la Torre et al. 2013) and the fine mapping of the CW at an epoch when the Universe was about half its current age.

In this paper, we exploit the final, complete sample of VIPERS to detect the filamentary structure of the CW at high redshift and to study the correlation between galaxy properties and their distance to the closest filament. After describing the data in Section 2, we illustrate in Section 3 the filament reconstruction with the Discrete Persistent Structure Extractor (DISPERSE; Sousbie 2011) on mock samples of VIPERS and its fidelity. We present the application to the VIPERS data in Section 4, where we also report a significative mass and type segregation within filaments. Finally, we discuss in Section 5 our results within the current paradigm of galaxy assembly. Unless stated otherwise, we assume the Planck Collaboration XIII (2015) cosmology with $H_0 = 67.51$ km s^{-1} Mpc^{-1}, $h = H_0/100$, $\Omega_{\rm m} = 0.3121$, and $\Omega_\Lambda = 0.6879$.

[1] This intrinsic alignment is also a source of systematics affecting the cosmic shear signal (e.g. Chisari et al. 2015).

2 DATA

VIPERS is a magnitude-limited spectroscopic galaxy survey to $i_{AB} \leq 22.5$. It covers an overall footprint of about 16 and 8 deg^2 in the W1 and W4 fields of the CFHTLS-Wide imaging survey, respectively. VIPERS spectra were collected in low-resolution mode, $R = 230$, leading to a radial velocity error of $\sigma_{\rm v} = 175(1 + z_{\rm spec})$ km s^{-1}. The spectroscopic targets were preselected in a colour–colour space to remove galaxies below $z = 0.5$, which coupled with an optimized observing strategy provides an average effective sampling rate of about 40 per cent. We refer the reader to the survey description papers by Guzzo et al. (2014) and Garilli et al. (2014) and to the parallel paper by Scodeggio et al. (2016) for more details.

In this work, we use the final galaxy sample, described in the latter paper (the so-called PDR-2). We consider only the most secure redshifts, corresponding to quality flag $\geq$2 in the VIPERS grading scheme (confidence level, CL $>$ 97 per cent). The mean number density of galaxies, $\overline{n}(z)$, varies significantly at the redshift boundaries of the survey, due to the magnitude limit, the target sampling rate, and the colour selection (see de la Torre et al. 2013; Guzzo et al. 2014, for details). For this reason, we limit this analysis to the 50 980 galaxies in the range $0.5 \leq z \leq 0.85$, where the typical spatial resolution in terms of mean intergalaxy separation, $\langle D_z \rangle \sim \overline{n}(z)^{-1/3}$, is the highest ($7.7 < \langle D_z \rangle/{\rm Mpc} < 10$). These values are comparable with those of the GAMA survey (Driver et al. 2011, with $4.6 < \langle D_z \rangle/{\rm Mpc} < 8.8$ for $0.1 < z < 0.3$ and $r \leq 19.8$), and make VIPERS the first galaxy redshift survey well suited for studying the CW at high redshifts. The stellar masses for the objects in our sample and the classification between active and passive populations were derived according to Moutard et al. (2016b), on the basis of the SED-fitting analysis of the multiwavelength data collected in the VIPERS regions[2] (Moutard et al. 2016a).

3 DETECTING FILAMENTS IN THE VIPERS SURVEY

The DISPERSE *code.* In order to trace the CW in VIPERS, we rely on DISPERSE (see Sousbie 2011; Sousbie, Pichon & Kawahara 2011, for a complete description). DISPERSE identifies filaments as ridges in the density field (calculated using the Delaunay Tessellation Field Estimator, DTFE). DISPERSE uses the discrete Morse theory to extract critical points, where the gradient of the density field vanishes (e.g. maxima and saddle points), and the field lines connecting them. It then pairs the critical points in topological features, called 'critical pairs', using the persistent homology theory. The robustness of each feature (including the filaments) is assessed by the relative density contrast of its critical pair, the so-called persistence, which is chosen to pass a certain signal-to-noise ratio (S/N) threshold. The noise level is defined relative to the variance of persistence values obtained from random sets of points. Because DISPERSE is based on a topologically motivated algorithm, it is both very robust and flexible through the choice of the persistence threshold. Since it filters out the sampling noise, it enables an unsmoothed density field, more noisy but less biased, to be analysed. By construction, it is also multiscale: it builds a network which adapts naturally to the uneven sampling of observed catalogues. The persistence threshold is calibrated on mocks to account for the specific design of VIPERS. To prevent the spurious detection

[2] The VIPERS-MLS survey: http://cesam.lam.fr/vipers-mls/

Downloaded from https://academic.oup.com/mnras/article-abstract/465/4/3817/2420717 by guest on 10 July 2020

of filaments near the edges of the survey, DISPERSE encloses each field in a larger volume. New particles are added by interpolating the density field measured at the boundary of the survey (see e.g. Sousbie et al. 2011).

Tests on VIPERS mock galaxy catalogues. We test the performance of DISPERSE on an updated version of the VIPERS mock galaxy catalogues described in de la Torre et al. (2013) matching the VIPERS final geometry. The upgrades are described in the parallel paper by de la Torre (in preparation). The parent catalogues include all the galaxies down to the magnitude limit $i_{AB} = 22.5$ together with the correct selection function at $0.4 < z < 0.6$ due to the VIPERS colour pre-selection. The VIPERS-like catalogues are built from the parent ones with all the observational effects applied (i.e. pointing strategy, target sampling rate, gaps between VIMOS quadrants, photometric mask and random errors on redshift).

The impact of observational biases on the skeleton reconstruction can be assessed by comparing the skeletons obtained from the parent and the VIPERS-like mock catalogues. To quantify the differences between two skeletons, we define a pseudo-distance between the two skeletons to be compared. In practice, a skeleton S_a is composed by N_a short straight segments, s_a^i. We define the pseudo-distance from a skeleton S_a to a skeleton S_b, $D(S_a, S_b)$, as the probability distribution function (PDF) of the distances between each segment of S_a, s_a^i, and its closest segment in S_b, s_b^j (Sousbie et al. 2009). The distributions $D(S_a, S_b)$ and $D(S_b, S_a)$ are composed of N_a and N_b distances, respectively. There is no reason for the pseudo-distance $D(S_a, S_b)$ to be identical to $D(S_b, S_a)$. Indeed, the discrepancy between the two PDFs is related to the differences between the two skeletons.[3]

Fig. 1 presents the PDFs of the pseudo-distances obtained by comparing the skeletons $S_{\rm Par}$ and $S_{\rm VIP}$ measured from the Parent and VIPERS-like catalogues, respectively, in the redshift range $0.5 < z < 0.85$. In the upper panel, DISPERSE is run with a persistence threshold of 3σ in both catalogues. This threshold guarantees that less than 1 per cent of critical pairs are spurious, as tested on random field simulations (Sousbie 2011). $S_{\rm VIP}$ is reconstructed with less accuracy and detail due to the lower sampling. An estimate of the uncertainty in the location of the filaments is given by the modes of the PDFs which do not peak at distance $D \sim 0$ (corresponding to a perfect match between the segments of the two skeletons) but $D \sim 1.5$–2 Mpc (marked as vertical arrows). The asymmetry between $D(S_{\rm Par}, S_{\rm VIP})$ and $D(S_{\rm VIP}, S_{\rm Par})$ reflects the fact that $S_{\rm Par}$ (full sampling) has much more details (i.e. the leaves of branches, or small branches) which have no counterpart in $S_{\rm VIP}$. On the other hand, 90 per cent of the segments of $S_{\rm VIP}$ have a counterpart in $S_{\rm Par}$ with distances $D \leq 10$ Mpc, illustrating the small fraction of spurious filaments. We also report the average length of the VIPERS-like ($L_{\rm VIP}$) and the Parent ($L_{\rm Par}$) skeletons, defined as the total skeleton length divided by the survey volume (expressed in Mpc Mpc^{-3}). $L_{\rm VIP}$ is shorter than $L_{\rm Par}$ as expected for a skeleton with fewer details. In the lower panel, the persistence threshold on the Parent catalogue is increased to 5.5σ. The length, $L_{\rm Par}$, is shortened with only the most significant filaments still present. The two PDFs for $D(S_{\rm VIP}, S_{\rm Par})$ and $D(S_{\rm Par}, S_{\rm VIP})$ are now much closer in amplitude and shape. Most of the segments in $S_{\rm Par}$ (75 per cent) have a counterpart in $S_{\rm VIP}$ with $D \leq 10$ Mpc. The modes of the distributions are almost unchanged. Even if the two skeletons are more similar, the skeleton $S_{\rm VIP}$ tends to oscillate around its true location (as reconstructed by $S_{\rm Par}$), making the length $L_{\rm VIP}$ longer than $L_{\rm Par}$.

[3] Note that by construction the Delaunay tessellation provides a simple way to reconnect LSS features with smoothed variations in density such as filaments across large gaps (Aragon-Calvo et al. 2015). For this reason and based on the results on simulations discussed here, we do not apply any correction for the gaps in the VIPERS survey.

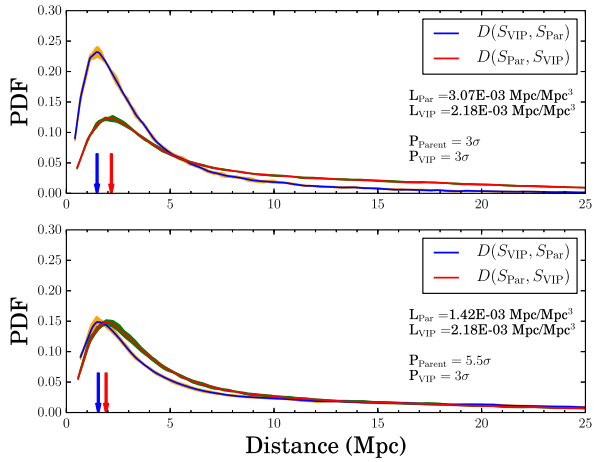

Figure 1. PDFs of the pseudo-distances (defined in Section 3) between the Parent and VIPERS-like skeletons. Blue lines and orange shaded areas refer to $S_{\rm VIP}$ projected on to $S_{\rm Par}$, while red lines and green shaded areas are the reverse. Solid lines correspond to the mean of 10 mocks and the shaded areas enclose the 1σ rms (note that uncertainties are negligible). Arrows show the modes of the distributions. Top panel: The two skeletons are extracted with a 3σ persistence threshold. Bottom panel: $S_{\rm Par}$ is extracted with a 5.5σ threshold.

In conclusion, the close match between the two PDFs indicates that the skeleton reconstructed at 3σ for the VIPERS-like catalogue is able to detect the most robust filaments (corresponding to a 5.5σ persistence threshold in a fully sampled data set) and contains a small fraction of spurious filaments.

4 RESULTS

The filamentary structures of the CW. We run DISPERSE on the VIPERS fields with a 3σ persistence threshold. Fig. 2 shows the filamentary network (green lines) for W1 (top panels) and W4 (bottom panels) fields, overplotted on a map of the density contrast $\delta = n_{\rm DTFE}/\overline{n}(z) - 1$, where $n_{\rm DTFE}$ is the local DTFE density estimate. Even in the 2D projections, we can see that filaments reveal the ridges of the 3D density field, which, by construction, connect the density peaks between them via saddle points. The averaged lengths of the skeletons are similar with $L \sim 0.0013$ and 0.0016 Mpc Mpc^{-3} in W1 and W4, respectively. At low ($z \leq 0.5$) and high redshifts ($z \geq 0.85$), the number of filaments drops as a consequence of the lower sampling, and only the most secure filaments are detected, as expected with DISPERSE. Thanks to the large contiguous volume probed by VIPERS, large voids, partly delineated by the filaments, are visible in both fields with radii as large as $R \sim 30$ Mpc (see Micheletti et al. 2014 and the parallel paper by Hawken et al. (2016) for void analysis in VIPERS).

Mass segregation inside filaments. We now investigate how different galaxy populations are distributed within this filamentary network in the redshift range $0.5 \leq z \leq 0.85$. We measure the distance of each galaxy to the nearest filament, $D_{\rm skel}$ (which, in the figure, we report normalized to $\langle D_z \rangle$ to take care of the variations of the mean intergalaxy separation across the redshift range considered). The normalized PDFs of the distances, in the W1 and W4 fields

Downloaded from https://academic.oup.com/mnras/article-abstract/465/4/3817/2420717 by guest on 10 July 2020

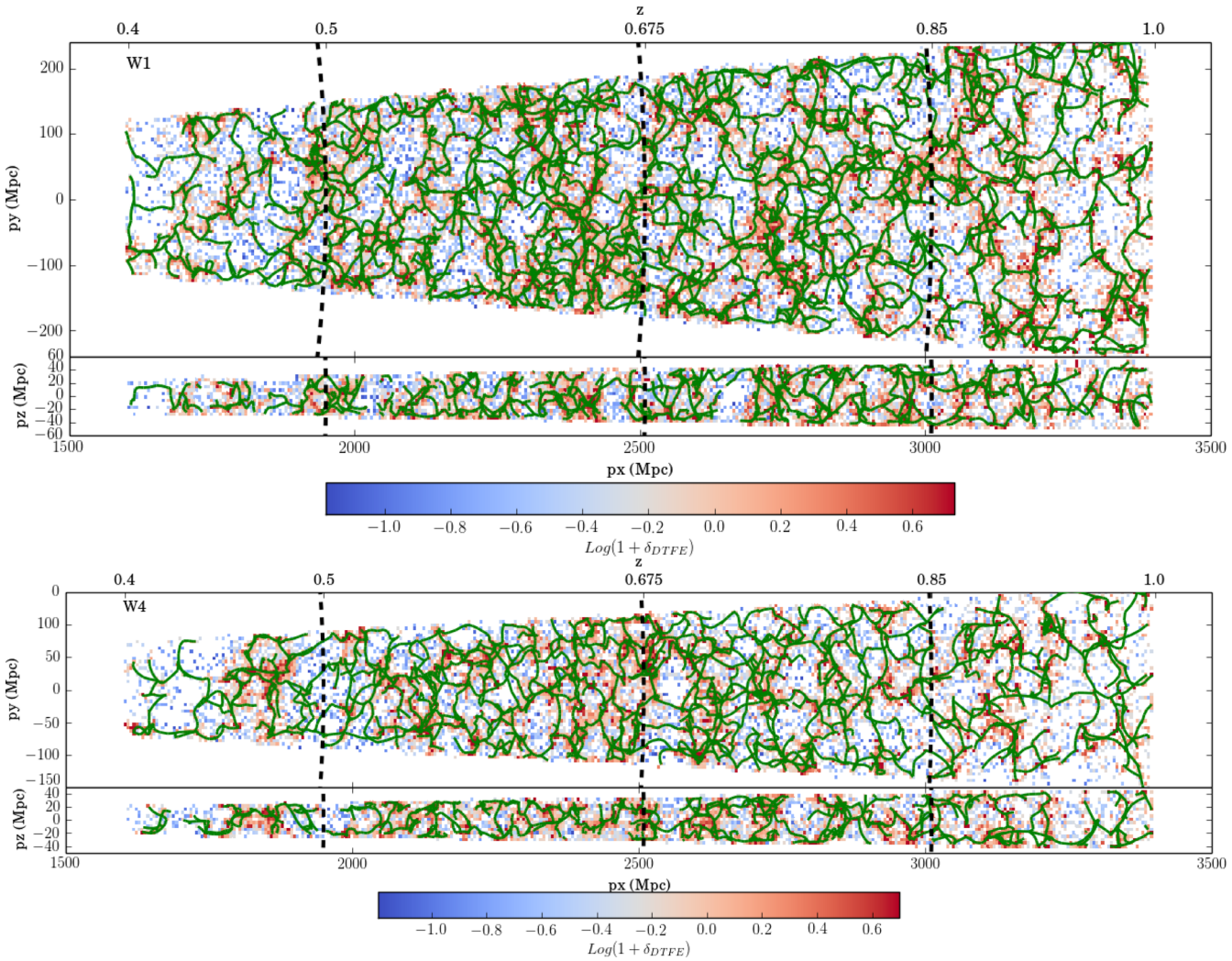

Figure 2. Projected distribution of the filaments reconstructed with DISPERSE (in dark green) in the VIPERS W1 (top panel) and W4 (bottom panel) fields in the range of $0.4 \leq z \leq 1$. The density contrast, $\log(1+\delta_{\rm DTFE})$, is averaged on cells of 5×5 Mpc^2 and colour-coded as indicated (white for empty cells). Top rows: projected distribution along the declination direction ($\Delta\delta = 2$). Bottom rows: projected distribution along the right ascension direction (in the central regions with $\Delta\alpha = 2$). 3D movies are available on the VIPERS website.

combined, are shown in Fig. 3 for three selections: low- versus high-mass galaxies, star-forming versus quiescent galaxies, and star-forming galaxies in three mass bins. The error bars are estimated with a block-wise (1 deg^2) jackknife resampling. The first two samples are limited to $M^* \geq 10^{10.5}\,{\rm M}_\odot$ to be complete in stellar mass for both quiescent and star-forming galaxies (see Davidzon et al. 2016), while a mass cut of $M^* \sim 10^{10}\,{\rm M}_\odot$ is used when only star-forming galaxies are considered.

A trend between distance and stellar mass is observed (left-hand column), with more massive galaxies being closer to filaments as indicated by the shift in the median values of the two PDFs (downward arrows). Passive galaxies are also found to be closer to filaments (middle column). While a large fraction (47 per cent) of our massive ($M^* \geq 10^{10.5}\,{\rm M}_\odot$) galaxies are also passive, by looking at the star-forming population alone, we observe a similar trend, albeit weaker, with the most massive star-forming galaxies being closer to filaments (right-hand column). However, since we wish to evaluate the impact of the filaments on galaxy properties, we have to take into account the contribution of the nodes of the density field, usually related to galaxy groups and clusters, which are at the intersections of filaments and are known to be privileged regions where quenching is more efficient. This task is not easy, as there are partial overlaps between the local density and the CW environment (Aragón-Calvo et al. 2010). As proposed by Gay et al. (2010), to minimize the node contributions, we weight each galaxy by the inverse of the density field smoothed using a Gaussian filter with $\sigma = 3$ Mpc. The weighted PDFs are shown in the middle row of Fig. 3. A shift in the medians of the PDFs to larger distances is observed, but the trends remain. We also adopted alternative approaches by rejecting galaxies in high-density regions ($\delta \geq 4$), located within groups, according to a parallel analysis (Iovino et al., in preparation), or by keeping only the filaments with a higher persistence threshold. They do not qualitatively change the results discussed in this section.

The significance of the observed trends is illustrated by the residuals between the weighted distributions expressed in units of σ (bottom row of Fig. 3). The deviations exceed 2σ in most of the bins except for star-forming samples alone (due to shot noise in the most massive bin). We also quantify the differences with the χ^2 test of independence and the probabilities of observing such a difference by chance, which are negligible (listed in middle panels). This confirms the existence of a weak but statistically significant

Downloaded from https://academic.oup.com/mnras/article-abstract/465/4/3817/2420717 by guest on 10 July 2020

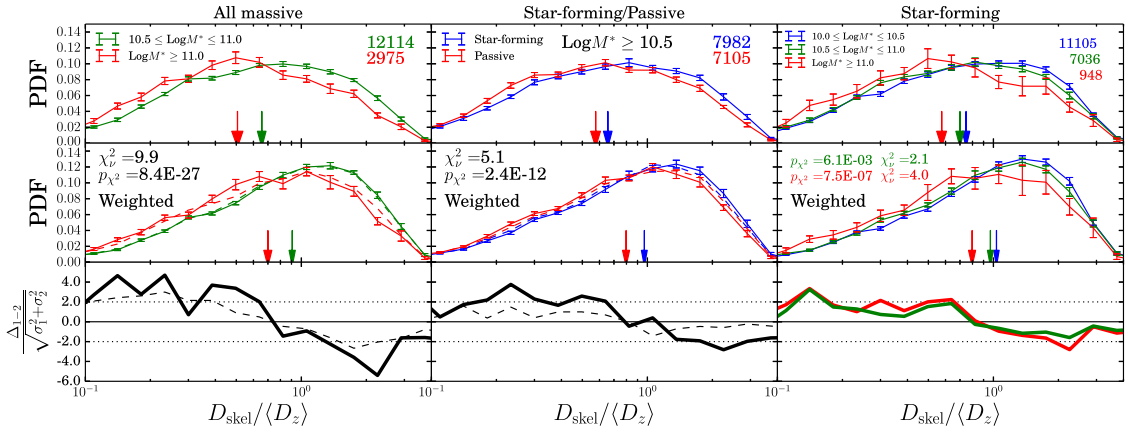

Figure 3. Distributions of the unweighted (top row) and density-weighted (middle row) normalized distances ($D_{\mathrm{skel}}/\langle D_z \rangle$), for three selections: low- versus high-mass galaxies (left-hand column), quiescent versus star-forming galaxies (middle column) and star-forming galaxies in three mass bins (right-hand column). Vertical arrows indicate the medians of the PDFs, and error bars represent the dispersions computed with block-wise jackknife resampling. The PDFs after reshuffling of the samples (see text) are shown with dashed lines. The differences between the weighted distributions are shown in the bottom row. For star-forming galaxies (right-hand panel), only the differences between high-intermediate (green) and high-low (red) mass bins are shown. The values resulting from the χ^2 test of independence are reported in the middle panels.

segregation effect inside the filaments and suggests that galaxy processing happens also during the drift of galaxies towards the nodes of the CW.

In Fig. 3, we also look at how the mass–density relation is hidden in the observed mass segregation. We split the sample in local density bins and reshuffle the stellar masses between the galaxies in each bin. The mean PDF distributions for 10 random reshufflings are shown as dashed lines on the middle left-hand panel. The PDFs for the low- and high-mass bins are close to the original ones, which shows that the mass segregation exists even after reshuffling the masses, if the mass–density relation is preserved. Therefore, the mass segregation inside the filaments emerges naturally from the mass–density relation and the anisotropic distribution of the density in the CW.

A similar approach is adopted for the galaxy-type segregation. We randomly attribute a galaxy type (passive/star forming) to galaxies by conserving the type fraction observed in different stellar mass bins. The mean PDFs for 10 random reshufflings are shown as dashed lines (middle panel). In this case, the segregation almost vanishes, with a difference between the two PDFs of less than 1σ. The observed type segregation therefore does not arise just from the mass–type fraction relation but could have its origin in the dynamic of the large-scale anisotropic structures of the CW.

5 DISCUSSION AND CONCLUSIONS

We reported the first characterization of large-scale filamentary structures at $z \sim 0.7$, carried out in the cosmological volume probed by the VIPERS spectroscopic survey. The reconstruction is based on the DISPERSE code and the capability of VIPERS to capture such a CW's filamentary network is tested on simulations. We observe a small but significant trend for galaxies with different stellar masses and stellar activity to segregate near the filaments with the most massive and/or passive galaxies being closer to filaments. The signal persists even after downweighting the contribution of nodes and high-density regions.

The galaxy segregation quantified in this paper is a first step in support of a new paradigm in galaxy formation where large-scale cosmic flows play a role in shaping galaxy properties. Beyond the observed anisotropy of the mass distribution (which follows naturally from the mass–density relation and the anisotropy of density in the CW), we expect that other physical parameters (e.g. stellar activity controlled in part by gas accretion or morphology and size controlled in part by angular momentum) will be impacted by this large-scale environment. Indeed, our results are fully consistent with the ingredients of the spin alignment theory presented in Codis et al. (2015), which relies on these large-scale cosmic flows. The stellar activity segregation observed here can be interpreted inside this theory. Low-mass or star-forming galaxies are preferentially located at the outskirts of filaments, a vorticity-rich environment (Laigle et al. 2015), where galaxies acquire both their angular momentum (leading to a spin parallel to the filaments) and their stellar mass essentially via smooth accretion (Welker et al. 2015). The stellar-mass segregation observed here is the next step, where at a higher mass, a transition is predicted in simulations, when more massive post-mergers drifting along filaments convert the orbital momentum of their progenitors into spin perpendicular to the axis of the filament, with increased efficiency for a higher merger rate (Dubois et al. 2014; Welker et al. 2015). The most massive galaxies, dominated by the quiescent population, should preferentially complete their stellar mass assembly in the core of filaments by merging.

We plan to extend the characterization of the CW in VIPERS in a future paper. It will be of interest to extend our analysis to other physical quantities such as SF rate or specific SF rate, spin orientation and extent to different CW perspectives: the distance to nodes within the filaments or, of particular interest, the distance from the saddle of the filaments, expected to be the region in the filament where galaxies have been the less affected by environmental effects. This will become within reach with the upcoming large and deep spectroscopic surveys such as PFS (Prime Focus Spectrograph). With its higher sampling and high-redshift extension ($z \sim 1.5$–2), the PFS-deep survey will offer the opportunity to explore such dependencies near the peak of the cosmic SF activity with an unprecedented accuracy.

Meanwhile, alternative approaches based on large multiband photometric surveys (e.g. COSMOS, J-PAS; Benitez et al. 2014) with accurate photometric redshifts allow us to analyse the

Downloaded from https://academic.oup.com/mnras/article-abstract/465/4/3817/2420717 by guest on 10 July 2020

projected 2D CW in narrow redshift slices. Preliminary results on the filamentary structures in the COSMOS field yield consistent results for the mass segregation inside the filaments (Laigle et al., in preparation).

ACKNOWLEDGEMENTS

This work is based on observations collected at the European Southern Observatory, Cerro Paranal, Chile, using the Very Large Telescope under programmes 182.A-0886 and partly 070.A-9007. Also based on observations obtained with MegaPrime/MegaCam, a joint project of CFHT and CEA/DAPNIA, at the Canada–France–Hawaii Telescope (CFHT), which is operated by the National Research Council (NRC) of Canada, the Institut National des Sciences de l'Univers of the Centre National de la Recherche Scientifique (CNRS) of France, and the University of Hawaii. This work is based in part on data products produced at TERAPIX and the Canadian Astronomy Data Centre as part of the Canada–France–Hawaii Telescope Legacy Survey, a collaborative project of NRC and CNRS. The VIPERS web site is http://www.vipers.inaf.it. This research is carried out within the framework of the Spin(e) collaboration (ANR-13-BS05-0005, http://cosmicorigin.org). NM acknowledges the financial contributions by grants ASI/INAF I/023/12/0 and PRIN MIUR 2010-2011 'The dark Universe and the cosmic evolution of baryons: from current surveys to Euclid'.

REFERENCES

Alpaslan M. et al., 2015, MNRAS, 451, 3249
Alpaslan M. et al., 2016, MNRAS, 457, 2287
Aragón-Calvo M. A., van de Weygaert R., Jones B. J. T., van der Hulst J. M., 2007, ApJ, 655, L5
Aragón-Calvo M. A., Platen E., van de Weygaert R., Szalay A. S., 2010, ApJ, 723, 364
Aragon-Calvo M. A., Weygaert R. v. d., Jones B. J. T., Mobasher B., 2015, MNRAS, 454, 463
Benitez N. et al., 2014, in Cenarro A. J., Figueras F., Hernández- Monteagudo C., Trujillo Bueno J., Valdivielso L., eds, Highlights of Spanish Astrophysics VIII, p. 148
Beygu B., Kreckel K., van de Weygaert R., van der Hulst J. M., van Gorkom J. H., 2013, AJ, 145, 120
Bond J. R., Kofman L., Pogosyan D., 1996, Nature, 380, 603
Chisari N. et al., 2015, MNRAS, 454, 2736
Codis S., Pichon C., Devriendt J., Slyz A., Pogosyan D., Dubois Y., Sousbie T., 2012, MNRAS, 427, 3320
Codis S., Pichon C., Pogosyan D., 2015, MNRAS, 452, 3369
Colless M. et al., 2001, MNRAS, 328, 1039
Davidzon I. et al., 2016, A&A, 586, A23
de la Torre S. et al., 2013, A&A, 557, A54
Dekel A., Birnboim Y., 2006, MNRAS, 368, 2
Dekel A. et al., 2009, Nature, 457, 451
Dressler A., 1980, ApJ, 236, 351
Driver S. P. et al., 2011, MNRAS, 413, 971
Dubois Y. et al., 2014, MNRAS, 444, 1453
Eardley E. et al., 2015, MNRAS, 448, 3665
Garilli B. et al., 2014, A&A, 562, A23
Gay C., Pichon C., Le Borgne D., Teyssier R., Sousbie T., Devriendt J., 2010, MNRAS, 404, 1801
Guo Q. et al., 2011, MNRAS, 413, 101
Guzzo L. et al., 2014, A&A, 566, A108
Hahn O., Porciani C., Carollo C. M., Dekel A., 2007, MNRAS, 375, 489
Hawken A. J. et al., 2016, preprint (arXiv:1611.07046)
Kereš D., Katz N., Weinberg D. H., Davé R., 2005, MNRAS, 363, 2
Laigle C. et al., 2015, MNRAS, 446, 2744
Martínez H. J., Muriel H., Coenda V., 2016, MNRAS, 455, 127
Micheletti D. et al., 2014, A&A, 570, A106
Moutard T. et al., 2016a, A&A, 590, A102
Moutard T. et al., 2016b, A&A, 590, A103
Pichon C., Pogosyan D., Kimm T., Slyz A., Devriendt J., Dubois Y., 2011, MNRAS, 418, 2493
Planck Collaboration XIII, 2015, A&A, 594, A13
Scodeggio M. et al., 2016, preprint (arXiv:1611.07048)
Sousbie T., 2011, MNRAS, 414, 350
Sousbie T., Colombi S., Pichon C., 2009, MNRAS, 393, 457
Sousbie T., Pichon C., Kawahara H., 2011, MNRAS, 414, 384
Springel V., Frenk C. S., White S. D. M., 2006, Nature, 440, 1137
Tempel E., Stoica R. S., Saar E., 2013, MNRAS, 428, 1827
Trujillo I., Carretero C., Patiri S. G., 2006, ApJ, 640, L111
Welker C., Dubois Y., Devriendt J., Pichon C., Kaviraj S., Peirani S., 2015, preprint, (arXiv:1502.05053)
York D. G. et al., 2000, AJ, 120, 1579
Zehavi I. et al., 2005, ApJ, 630, 1
Zhang Y., Yang X., Wang H., Wang L., Mo H. J., van den Bosch F. C., 2013, ApJ, 779, 160

[1]*Dipartimento di Fisica e Astronomia (DIFA), Università di Bologna, v.le Berti Pichat 6/2, I-40127 Bologna, Italy*
[2]*CNRS, Laboratoire d'Astrophysique de Marseille, UMR 7326, Aix Marseille Université, F-13388, Marseille, France*
[3]*Institute d'Astrophysique de Paris, UMR7095 CNRS, Université Pierre et Marie Curie, 98 bis Boulevard Arago, F-75014 Paris, France*
[4]*Korea Institute of Advanced Studies (KIAS), 85 Hoegiro, Dongdaemun-gu, Seoul 02455, Republic of Korea*
[5]*INAF – Osservatorio Astronomico di Bologna, via Ranzani 1, I-40127 Bologna, Italy*
[6]*INAF – Osservatorio Astronomico di Brera, Via Brera 28, 20122 Milano, via E. Bianchi 46, I-23807 Merate, Italy*
[7]*Università degli Studi di Milano, via G. Celoria 16, I-20130 Milano, Italy*
[8]*INAF – IASF Milano, via Bassini 15, I-20133 Milano, Italy*
[9]*INAF – Osservatorio Astronomico di Torino, I-10025 Pino Torinese, Italy*
[10]*Laboratoire Lagrange, UMR7293, Université de Nice Sophia Antipolis, CNRS, Observatoire de la Cote d'Azur, F-06300 Nice, France*
[11]*Institute of Physics, Jan Kochanowski University, ul. Swietokrzyska 15, PL-25-406 Kielce, Poland*
[12]*National Centre for Nuclear Research, ul. Hoza 69, PL-00-681 Warszawa, Poland*
[13]*INFN, Sezione di Bologna, viale Berti Pichat 6/2, I-40127 Bologna, Italy*
[14]*Aix-Marseille Université, Jardin du Pharo, 58 bd Charles Livon, F-13284 Marseille cedex 7, France*
[15]*IRAP, 9 av. du colonel Roche, BP 44346, F-31028 Toulouse cedex 4, France*
[16]*Astronomical Observatory of the Jagiellonian University, Orla 171, PL-30-001 Cracow, Poland*
[17]*School of Physics and Astronomy, University of St Andrews, St Andrews KY16 9SS, UK*
[18]*INAF – IASF Bologna, via Gobetti 101, I-40129 Bologna, Italy*
[19]*INAF – Istituto di Radioastronomia, via Gobetti 101, I-40129 Bologna, Italy*
[20]*Aix Marseille Université, CNRS, CPT, UMR 7332, F-13288 Marseille, France*
[21]*Dipartimento di Matematica e Fisica, Università degli Studi Roma Tre, via della Vasca Navale 84, I-00146 Roma, Italy*
[22]*INFN, Sezione di Roma Tre, via della Vasca Navale 84, I-00146 Roma, Italy*
[23]*INAF – Osservatorio Astronomico di Roma, via Frascati 33, I-00040 Monte Porzio Catone (RM), Italy*
[24]*Astronomical Observatory of the University of Geneva, ch. d'Ecogia 16, CH-1290 Versoix, Switzerland*
[25]*INAF – Osservatorio Astronomico di Trieste, via G. B. Tiepolo 11, I-34143 Trieste, Italy*

This paper has been typeset from a TEX/LATEX file prepared by the author.

Downloaded from https://academic.oup.com/mnras/article-abstract/465/4/3817/2420717 by guest on 10 July 2020